Supplementary Figure captions

Figure S1. Sequence alignment of Rvb1 and Rvb2, Related to main Figure 1.

Amino acid sequences of Rvb1p and Rvb2p from six organisms including *Saccharomyces cerevisiae, Homo sapiens, Chaetomium thermophilum, Mus musculus, Danio rerio* and *Schizosaccharomyces pombe* are aligned to highlight structural features discussed in the text. Secondary structures determined from the crystal structure of *Chaetomium thermophilum* Rvb1/2 heterocomplex are labeled on top of the sequences. Arrows represent α-helix (α) and 3/10 helices (η), and cylinders represent β-strands (β). For Rvb1p, DI is colored dark green, DII_{EXT} is colored yellow, DII_{INT} is colored orange, and DIII is colored light green. For Rvb2p, DI is colored dark cyan, DII follows the same color code as shown in Rvb1p, and DIII is colored light cyan.

Figure S2. Purification of ScR2TP components, Nop58p, and ScR2TP Related to main Figures 1, 2, 3, 4, 5, and 7.

A. Purification and analysis of his-tagged Pih1p-Tahp1 complex. Left: gel-filtration UV absorbance profile for His-Pih1p-Tah1p. Right: Coomassie blue stained SDS-PAGE gel for purified Pih1p-Tah1p and each of the two Pih1p truncation mutants. "Ni elution" denotes sample from Ni-NTA elution and "Peak" denotes peak samples from gel filtration column. B. SDS-PAGE gels from the TEV protease-treatment of the His-tagged Rvb1/2p heterocomplex. The Ni-NTA eluate for co-purified His-Rvb1/2p was incubated with TEV protease to remove the His-tag. Comparison of "pre-cleavage" and "post-cleavage" indicates full digestion of His-tagged sample. C.

Purification and analysis of non-tagged Rvb1/2p. “Peak” indicates the single gel filtration elution peak. D. Purification and analysis of the Rvb2p-Pih1p-Tah1p complex ($R2_2TP$). Cells expressing His-tagged Pih1p-Tah1p were mixed with those expressing tag-free Rvb2p and subjected to affinity purification by Ni-NTA followed by size exclusion chromatography. Upper, gel-filtration UV absorbance profile for the $R2_2TP$ complex. Lower: Protein contents of the two peaks were examined with Coomassie Blue-stained SDS-PAGE gel. Fractions analyzed by SDS-PAGE are indicated by numbered arrows. Those corresponding to assembled $R2_2TP$ complex (between “2” and “3”) were used in subsequent structural analysis. E. Purification and analysis of His-tagged Nop58p_447. Left, S200 column elution profile, Right, SDS-PAGE gel analysis of the two major peaks. Rvb1/2p complex was included as a comparison. Both Peak 1 and Peak 2 were verified by western blotting to contain Nop58p_447 (data not shown). Peak 2 was used in cross-linking and AUC studies. F. Separately purified Pih1p-Tah1p and Rvb1/2p complexes were incubated overnight at 4 °C before being separated on a gel filtration column (left) and the elution fractions were analyzed by silver stained SDS-PAGE gel (right). Left, The UV absorption profiles for both mixed complexes and Rvb1/2p complex alone were compared to indicate formation of new species. Peaks labeled as “P1”, “P2”, and “P3” were analyzed on silver stained SDS-PAGE. Both peaks “P1” and “P2” contained all four proteins. However, “P2” was not present in either free Rvb1/2p or Pi1hp-Tah1p elution profiles and was shown in negative stain EM analysis to contain mostly hexameric species. Note that the peak P1 was shown by negative staining to contain primarily aggregated proteins and Rvb1/2p dodecamers. Thus, the presence

of bands corresponding to Pih1p and Tah1p in peak P1 may be a combined result of insufficient separation of the gel filtration column and the high sensitivity of silver staining.

Figure S3. EM analysis of the ScR2TP complex, Related to main Figures 3.

A. A representative micrograph of negatively stained ScR2TP particles. B. Flow chart describing three-dimensional classifications of the negatively stained ScR2TP particles. Numbers indicate the total number of particles belonging to each class represented by the electron density. The initial 3D model was obtained from the 3D structure of $R2_2TP$ complex low-pass filtered to 60 Å (see Fig. S4). C. A representative micrograph of ice-embedded ScR2TP particles. D. Flow chart describing the three-dimensional classification of the ScR2TP particles. Numbers indicate the total number of particles belonging to each class represented by the electron density. The final density used for structural analysis is that containing 4839 particles. Inset shows an end-on view of the electron density overlaid with the final refined Rvb1/2p structure. E. Particle orientation distributions for two of the three rotation angles in the last iteration of the structure refinement. F. Gold-standard Fourier shell correlation (FSC) of the final cryoEM map of the ScR2TP complex.

Figure S4. EM analysis of the nucleotide-bound ScR2TP complex, Related to main Figures 3.

Representative 2D averages of ADP- (+ADP) and ATP-treated (+ATP) ScR2TP used for cryoEM analysis were obtained from analyzing 4500-5000 negatively stained

particles imaged on a CM120 electron microscope equipped with a CCD detector. The percentages of top views were calculated from the fractions of top views with nearly symmetric rings ("rings") over the total number of classifiable particles. The remaining percentage is assigned to the "distorted rings/half-barrel" category that includes less perfect rings or in the case of ADP-treated ScR2TP very few half-barrel- like particles. The 2D averages of non nucleotide-treated ScR2TP (but incubated under the same condition as nucleotide-treated samples) obtained from particles collected on the Titan-Krios microscope equipped with a DE20 director electron detector are included for comparison. Note that no or nearly no prominent side views as those in non nucleotide-treated averages could be identified in the nucleotide-treated ScR2TP particles.

Figure S5. EM structural analysis of the negatively stained $R2_2TP$ complex, Related to main Figure 5.

A. A representative micrograph of negatively stained $R2_2TP$ particles. B. Flow chart outlining the three-dimensional classification of $R2_2TP$ particles. The initial model was obtained from the crystal structure of *Chaetomium thermophilum* Rvb1/2 phase randomized and low-pass filtered to 50 Å.

Figure S6. Mass spectrometry (MS) analysis of selected cross-linked peptides, Related to main Figure 7.

A. Orbitrap mass spectrum of peptide BS3 cross-linked between Rvb1p Lys177 and Pih1p Lys239. The mass difference (Δm) of 4.0252 Da between light (*d0*) and heavy

(*d4*) peptide pair confirms the peptide is indeed cross-linked. B. Collision-induced dissociation (CID) MS^2 of $[M+4H]^{4+}$ m/z 570.5639, peptides BS3-d0 cross-linked between Rvb1p Lys177 and Pih1p Lys239. The top panel shows the LTQ CID MS^2 spectrum of the peptides BS3 cross-linked between Rvb1p Lys177 and Pih1p Lys239. Peaks in blue are y ions, in green are y-H_2O or y-NH_3 ions, in red are b ions, and in pink are b-H_2O or b-NH_3 ions. The bottom left panel shows the deviations of observed fragment ions. The bottom right shows the sequence coverage. C. Orbitrap mass spectrum of peptide BS3 cross-linked between Pih1p Lys52 and Nop58p Lys393. The mass difference (Δm) of 4.0252 Da between light (*d0*) and heavy (*d4*) peptide pair confirms the peptide is indeed cross-linked. D. Collision-induced dissociation (CID) MS^2 of $[M+4H]^{4+}$ m/z 594.6629, peptides BS3-d0 cross-linked between Pih1p Lys52 and Nop58p Lys393. The top panel shows the LTQ CID MS^2 spectrum of the peptides BS3 cross-linked between Pih1p Lys52 and Nop58p Lys393. Peaks in blue are y ions, in green are y-H_2O or y-NH_3 ions, in red are b ions, and in pink are b-H_2O or b-NH_3 ions. The bottom panel shows the deviations of observed fragment ions. The right shows the sequence coverage.

Figure S7. Hydrogen-deuterium (H/D) exchange analysis, Related to main Figure 7.

A. Deuterium uptake profiles plotted as deuterium incorporation *versus* H/D exchange period (log_{10} scale) for selected Pih1p peptide segments from free Pih1p-Tah1p (blue) and its ScR2TP complex (red). Segments 19-37, 25-35 and 264-270 showed an decrease, whereas segments 23-34 and 71-93 exhibited an increase in

deuterium uptake upon ScR2TP formation. The deuterium update profiles of Pih1p segments 94-107, 306-312, and 328-337 are essentially unchanged upon binding to Rvb1/2p. Time-course deuterium incorporation levels (smooth curves) were generated by a maximum entropy fitting method based on a maximum of three different H/D exchange rate constants per peptide (Zhang, Z; Guan, S.; Marshall, A.G. *Protein Sci.* 1997 8, 2203–2217.). B. Averaged relative deuterium-uptake difference (ARDD) heat map ($ARDD=\sum_{i}\frac{\mathbf{Complex(ti)\text{-}Pih1p(ti)}}{\mathbf{Pih1p(ti)}}$) for free Pih1p-Tah1p and the ScR2TP complex. The color-coded relative deuterium-uptake level is shown below each proteolytic peptide. The deuteration level was calculated by averaging deuterium-uptake (D-uptate) for each amino acid in all proteolytic segments containing it. Residues are coded grey if no data are available or relative deuterium-uptake change is less than 10%. C. Deuterium incorporation *versus* H/D exchange period (log_{10} scale) for selected segments of Tah1p in free Pih1p-Tah1p and in its ScR2TP complex indicates increased deuterium update for Tah1p on binding to Rvb1/2p for segments 1-5, 18-25 and 31-44, and no change in deuterium uptake for 100-104. D. Averaged relative deuterium-uptake difference (ARDD) heat map for free Tah1p and in its ScR2TP complex, color coded as in B.

Table S1. Stoichiometry Identification by mass spectrometry, Related to main Figure 3.

Table S2. Intermolecular cross-linked residues, Related to main Figure 7.

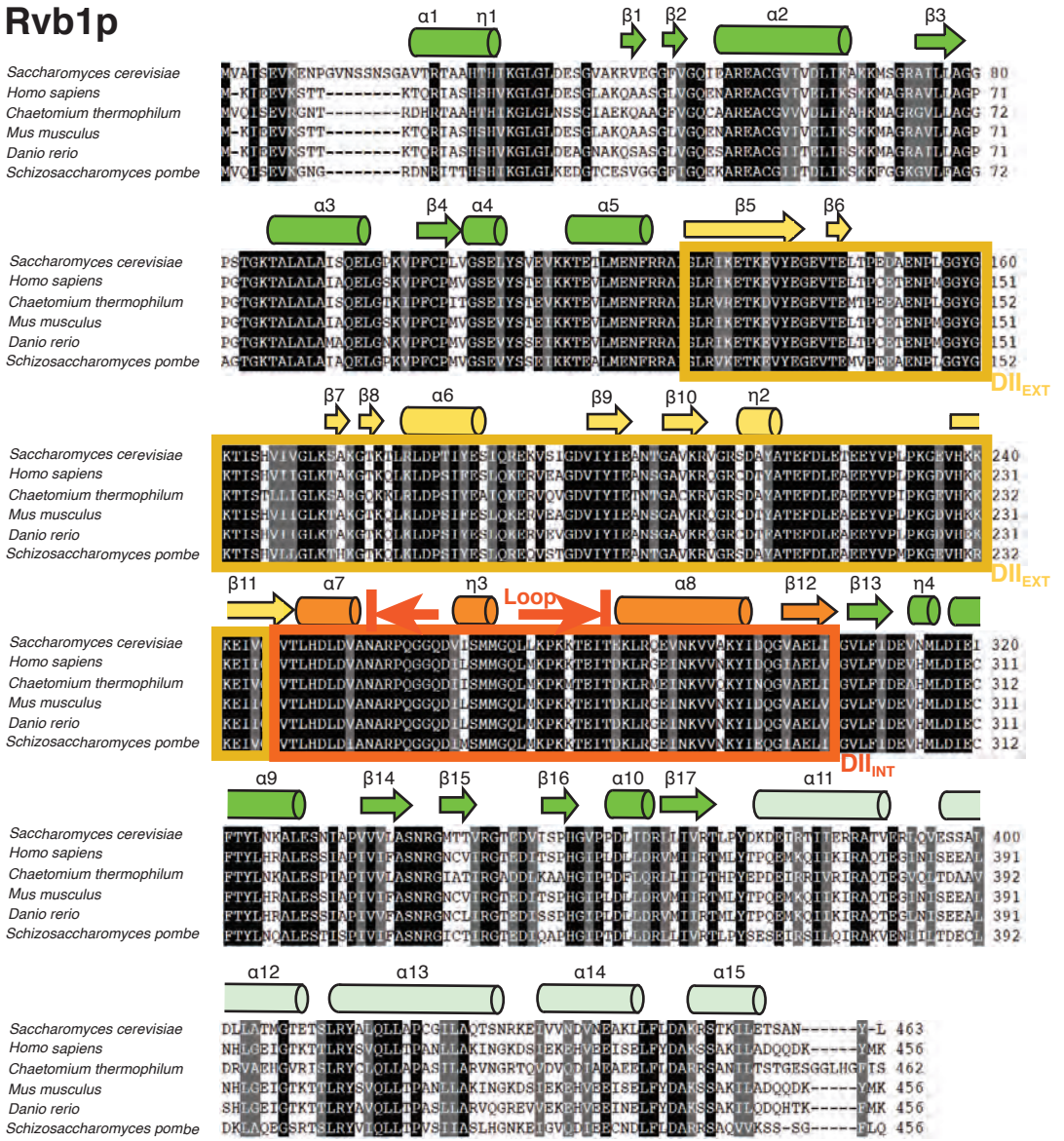

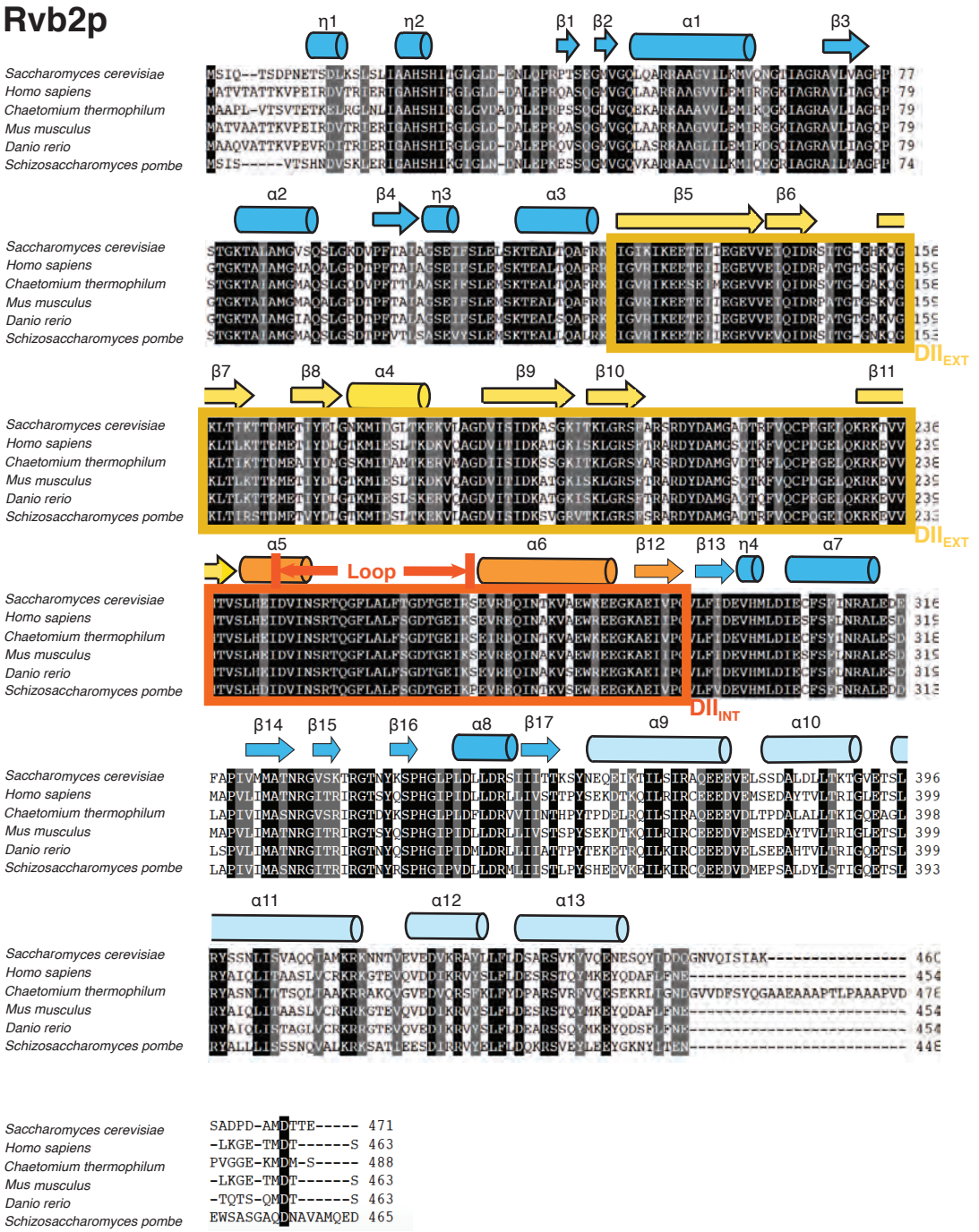

Tian et al. Fig. S1

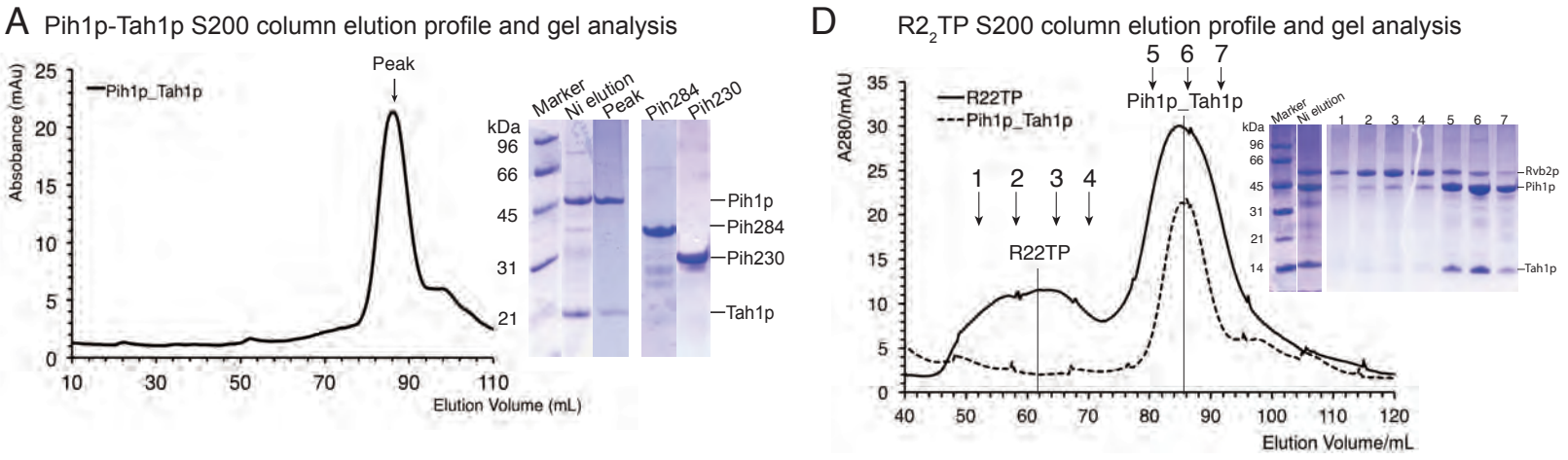

Tian et al., Fig. S2

A

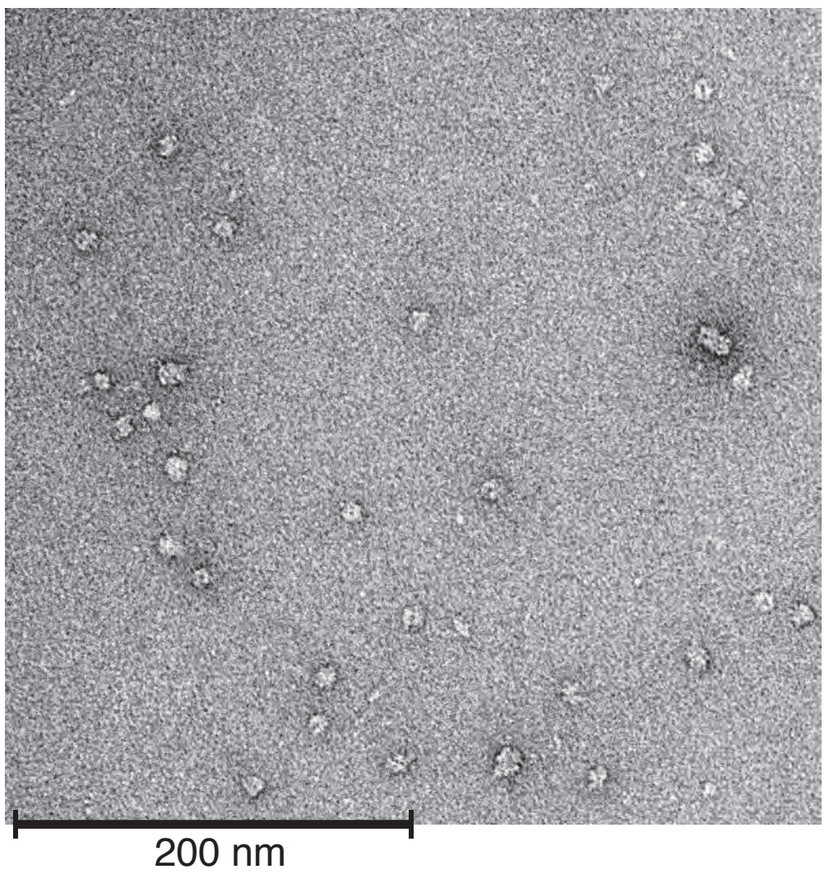

R2TP negative stain

B

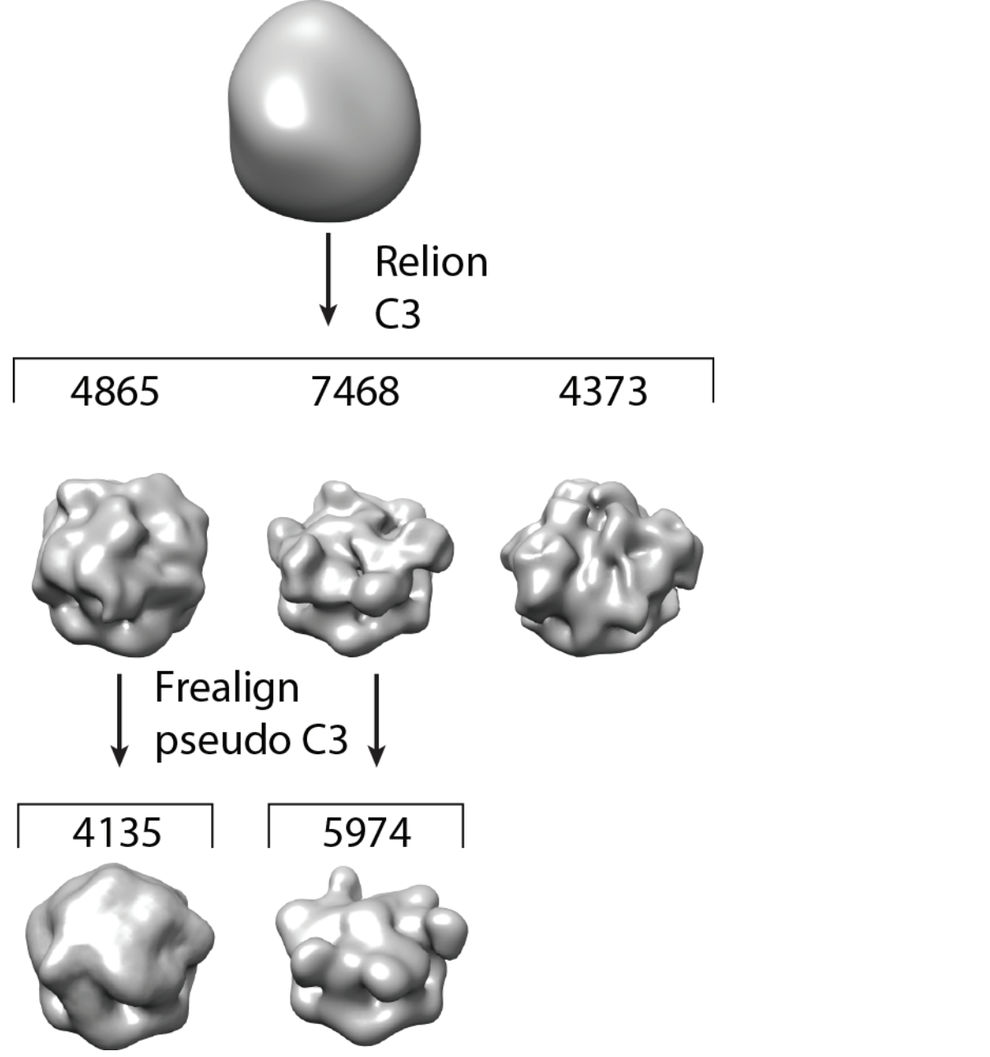

C

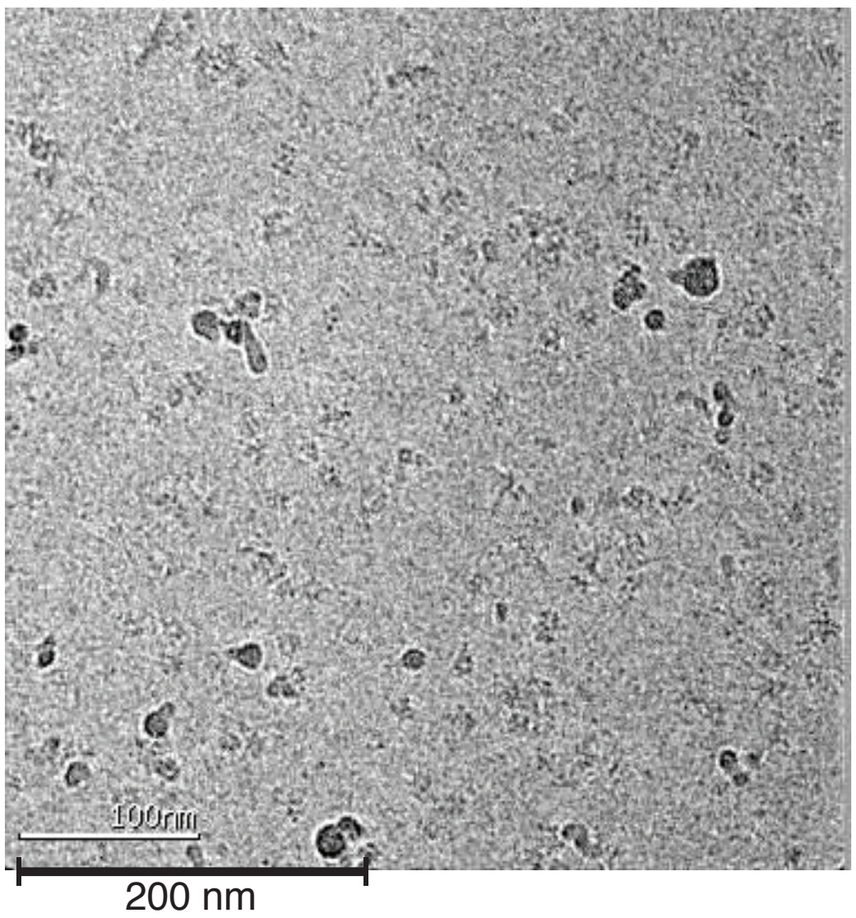

R2TP cryo

D

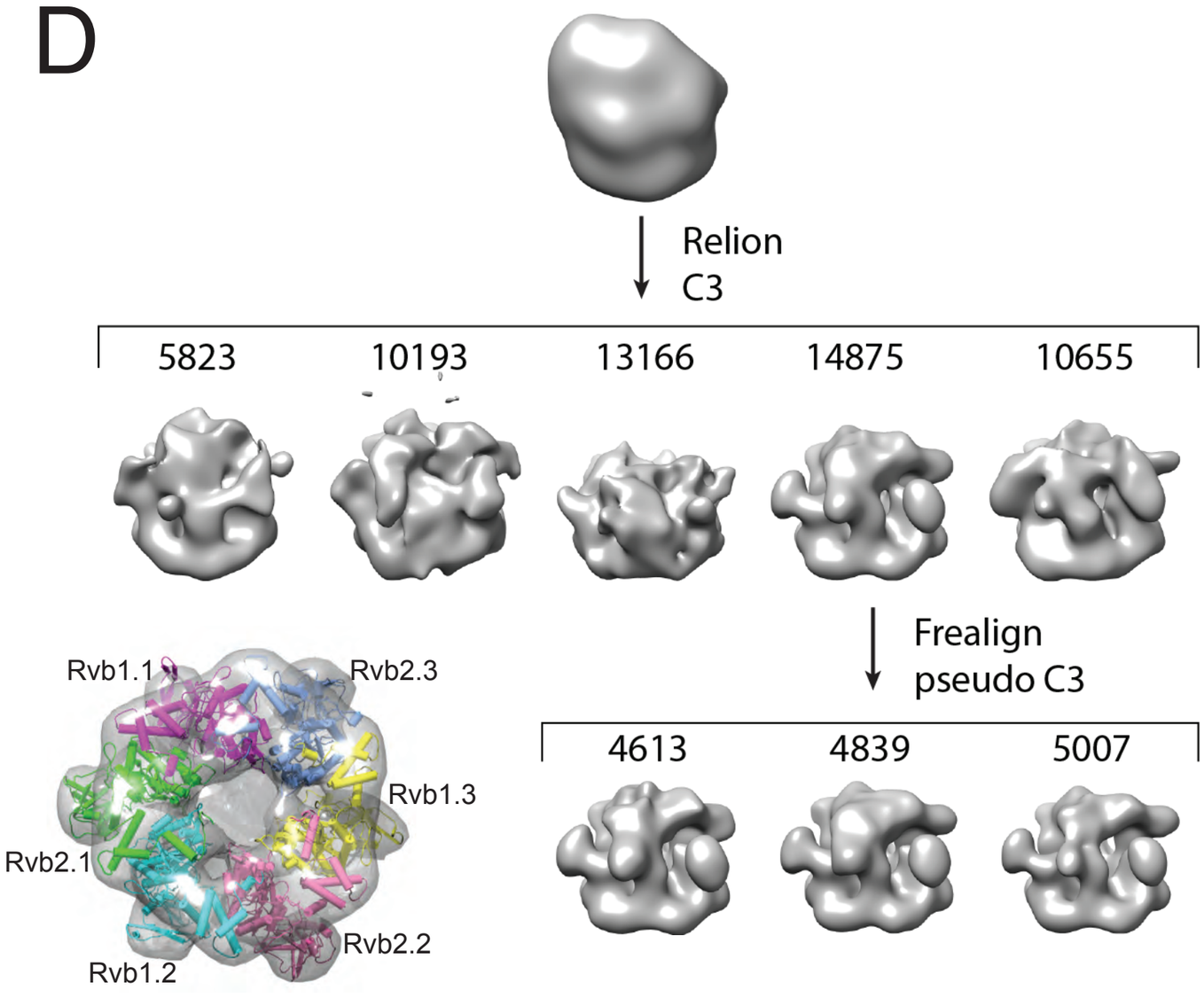

E

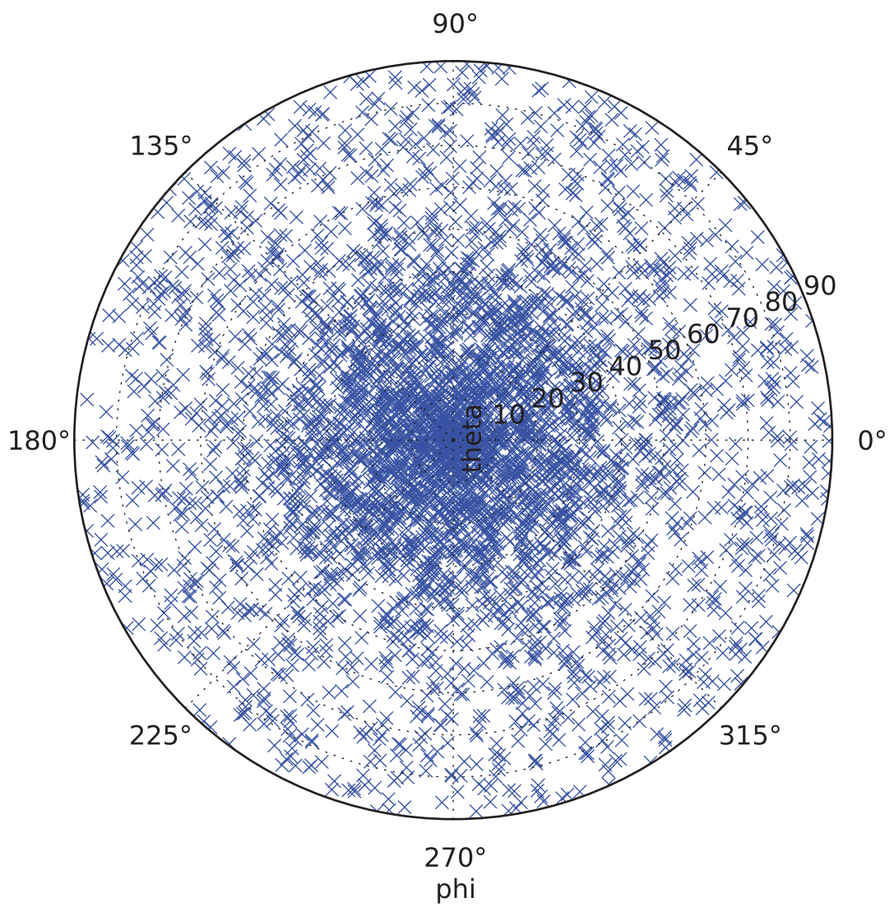

F

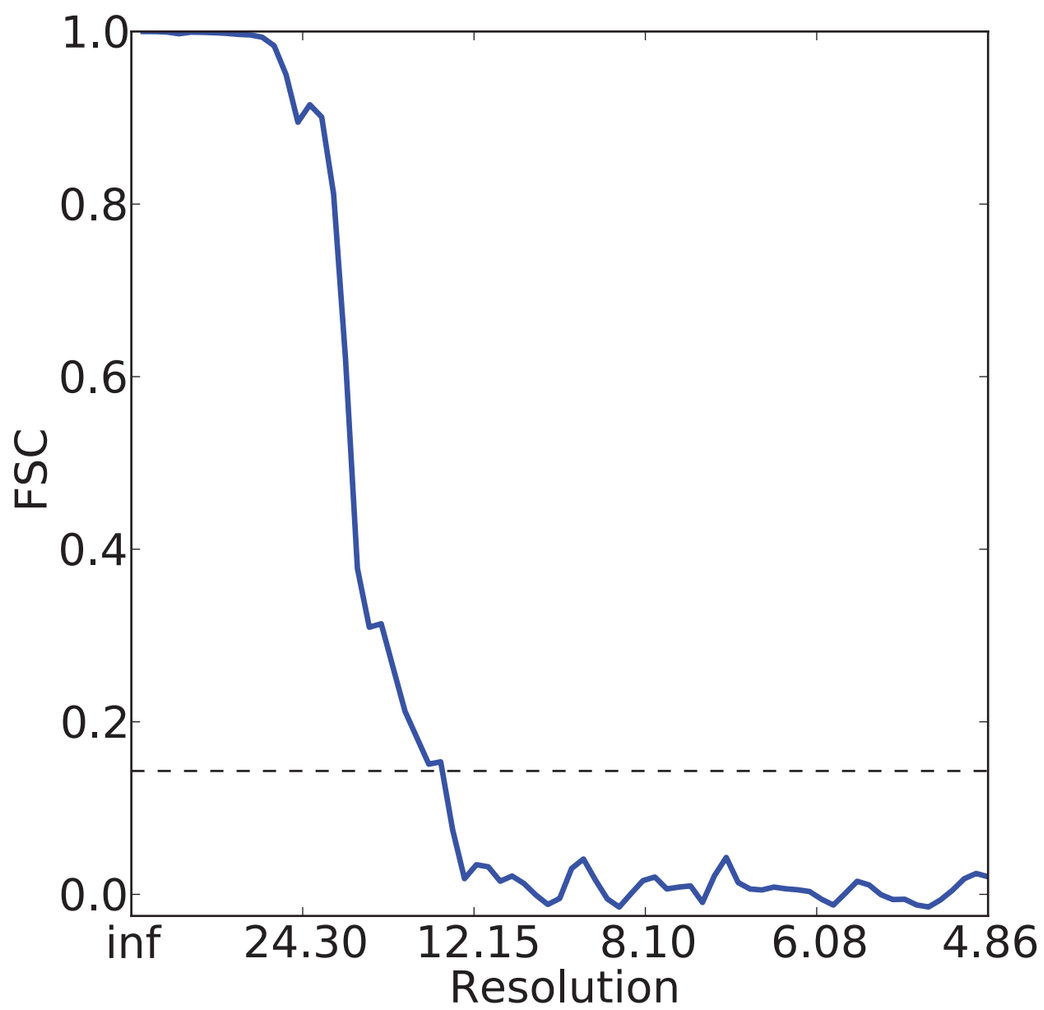

Tian et al., Fig. S3

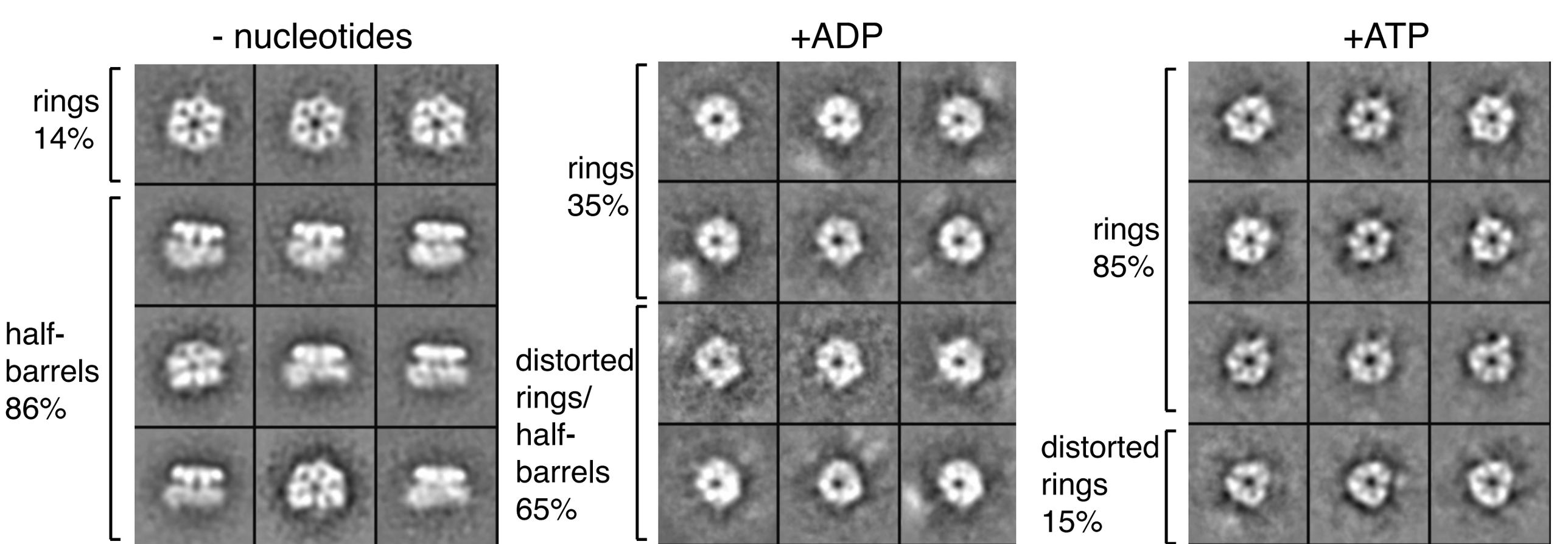

Tian et al., Fig. S4

A

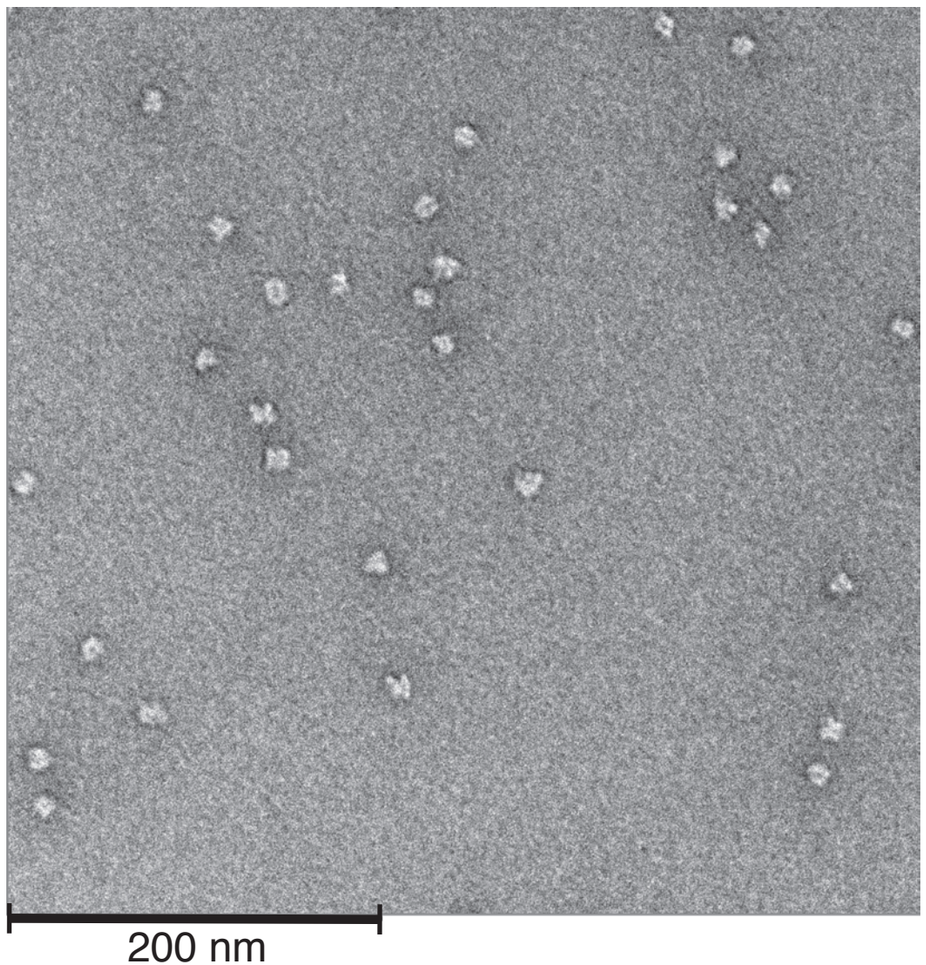

$R2_2TP$ negative stain

B

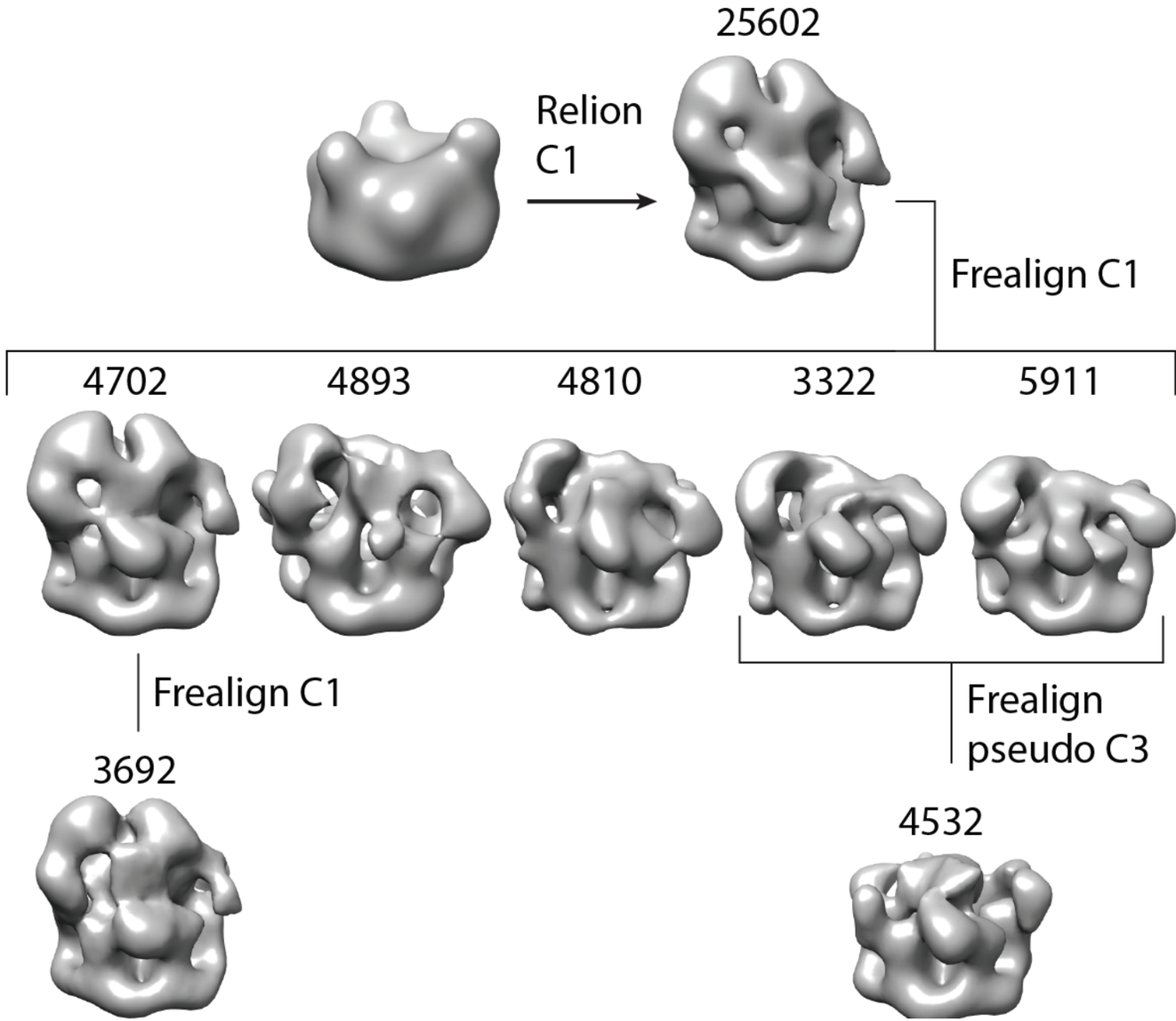

Tian et al., Fig. S5

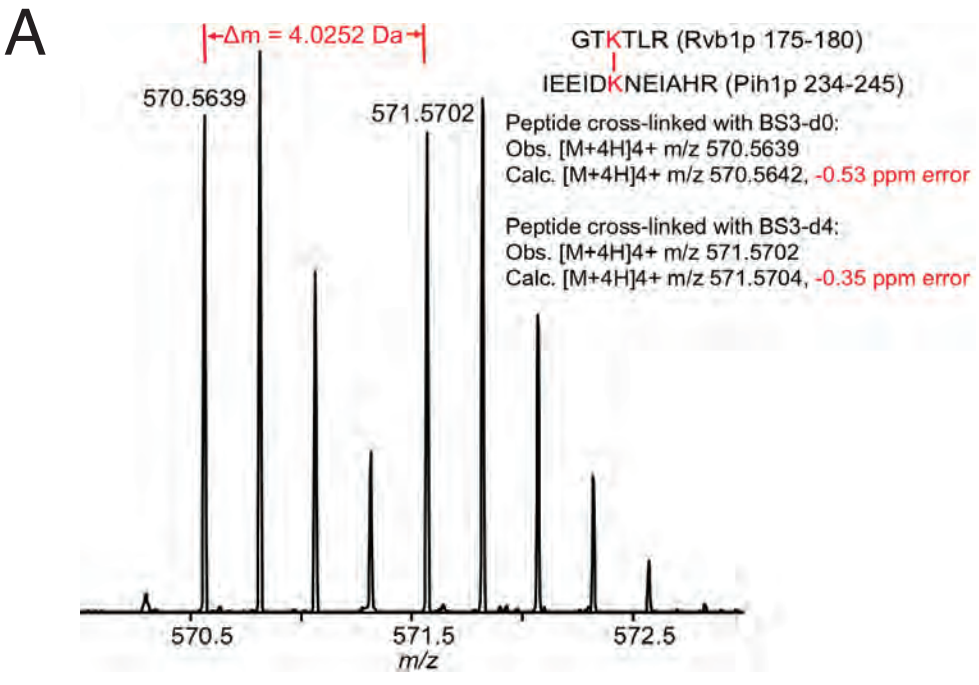

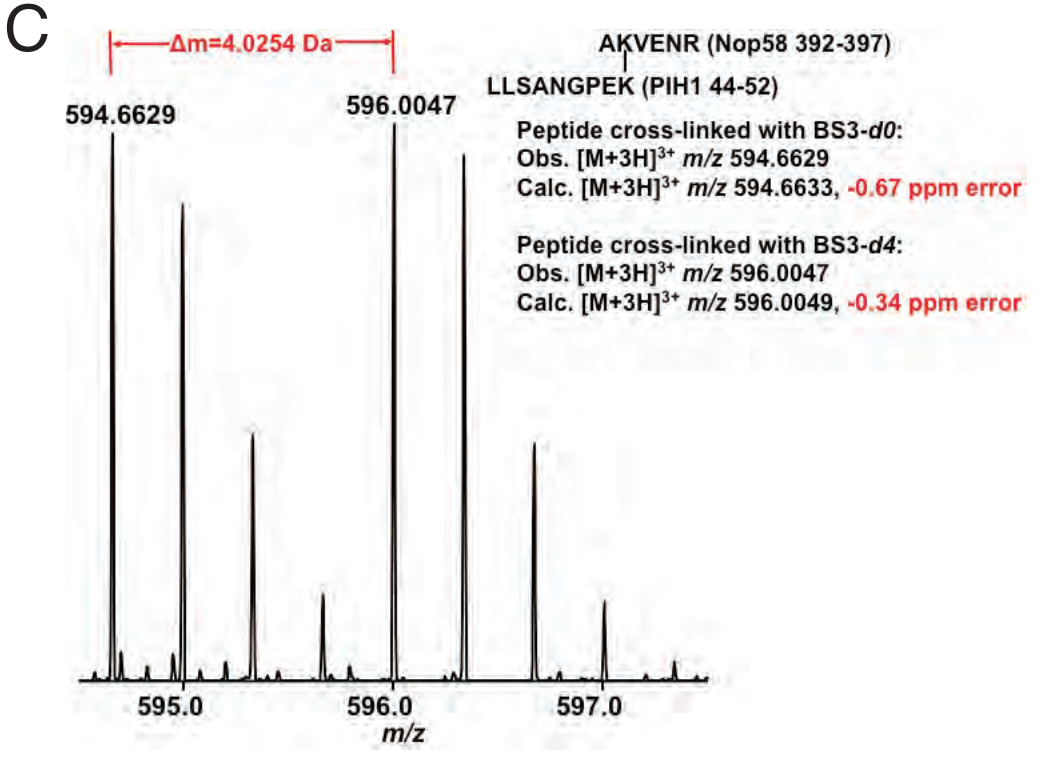

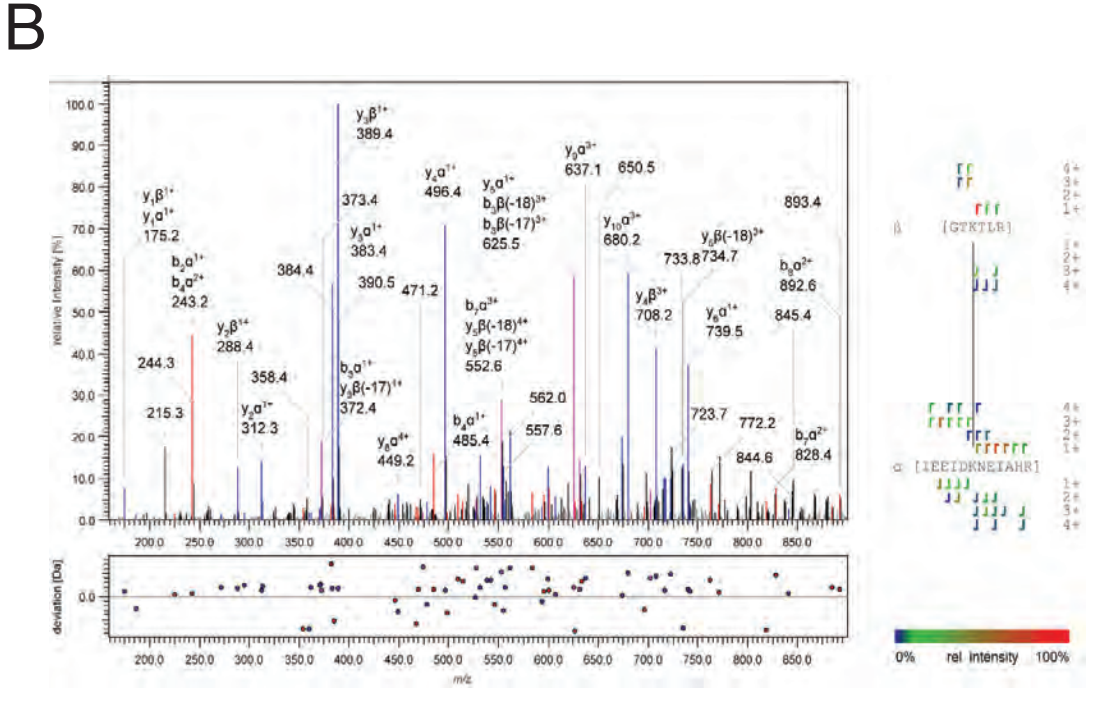

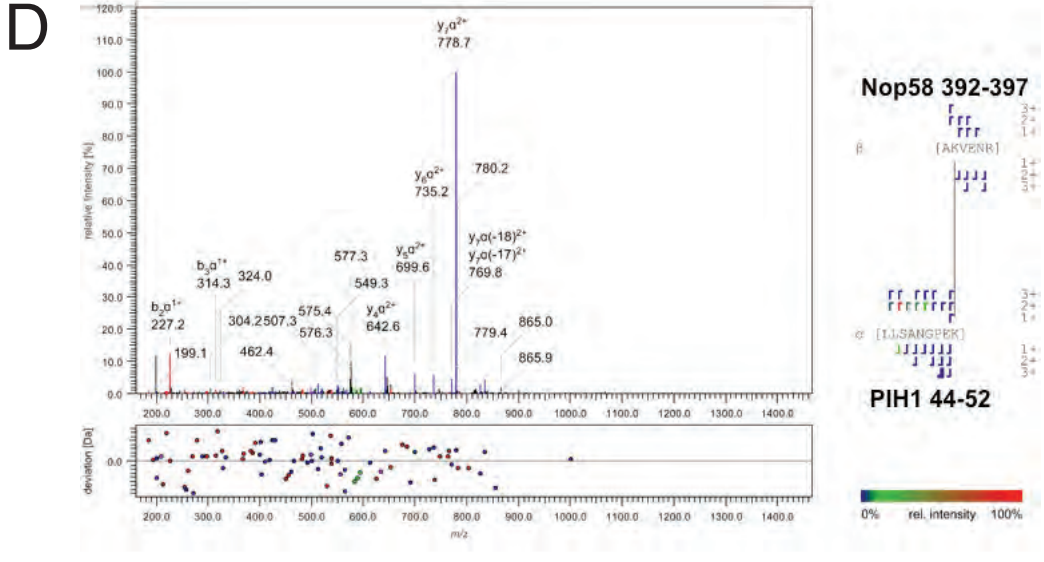

Tian et al., Fig. S6

A

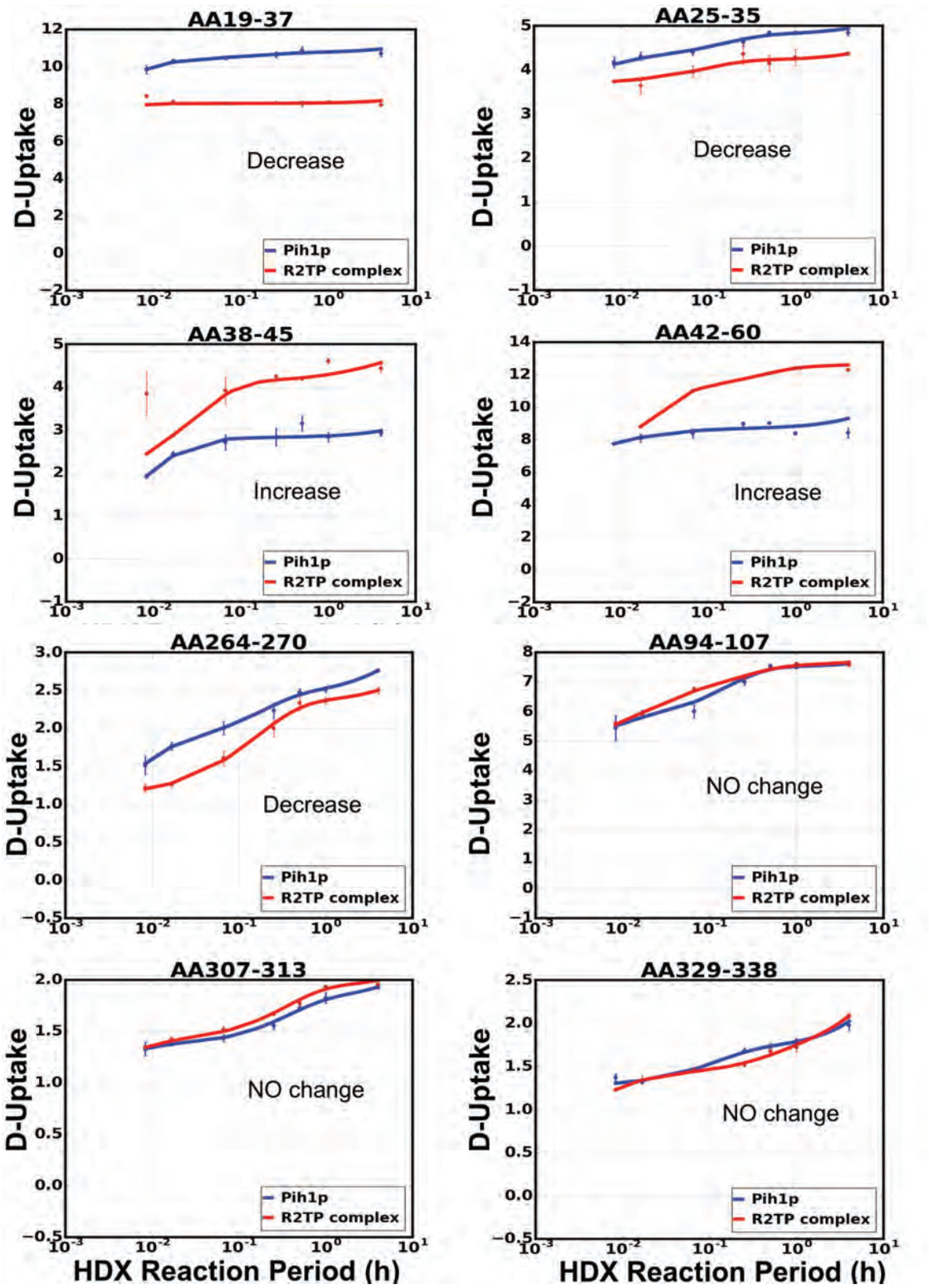

B

C

D

Tian et al., Fig. S7

Table S1. Stoichiometry identification by mass spectrometry*, Related to STAR Method Section "Stoichiometry and protein identification by mass spectrometry"

Protein	Accesion Number	Magnitude A (e+11)	Magnitude B (e+11)	Magnitude C (e+11)	Total Magnitude (e+11)	Ratio A	Ratio B	Ratio C	Average Ratio
Tah1p	P25638	0.994	0.891	0.992	2.88	1	1	1	1
Pih1p	P38768	2.99	3.2	3.16	9.35	3.015	3.59	3.18	3.25
Rvb1p	Q03940	5.71	5.69	5.81	17.2	5.74	6.39	5.86	5.98
Rvb2p	Q12464	5.82	5.55	5.71	17.1	5.86	6.22	5.75	5.93

*Ratios A, B, and C refer to ratios obtained from samples prepared in triplicate.

Table S2. Intermolecular cross-linked residues, Related to STAR Method section “Lysine-specific cross-linking coupled with mass spectrometry”

R2TP Cross-links

Protein1	Accession Number	Cross-linked Residue	Protein2	Accession Number	Cross-linked Residue	Score
Rvb1p	Q03940	Lys171	Pih1p	P38768	Lys239	155
Rvb1p	Q03940	Lys174	Pih1p	P38768	Lys18	162
Rvb1p	Q03940	Lys174	Pih1p	P38768	Lys248	170
Rvb1p	Q03940	Lys177	Pih1p	P38768	Lys239	181
Rvb2p	Q12464	Lys157	Pih1p	P38768	Lys10	166
Rvb2p	Q12464	Lys183	Pih1p	P38768	Lys275	151
Rvb2p	Q12464	Lys198	Pih1p	P38768	Lys10	150
Pih1p	P38768	Lys293	Tah1p	P25638	Ser78	150
Rvb1p	Q03940	Lys432	Rvb2p	Q12464	Lys59	156
Rvb1p	Q03940	Lys450	Rvb2p	Q12464	Lys331	195
Rvb1p	Q03940	Lys450	Rvb2p	Q12464	Thr335	171
Rvb1p	Q03940	Lys454	Rvb2p	Q12464	lys331	197
Rvb1p	Q03940	Lys454	Rvb2p	Q12464	Thr335	194
Rvb1p	Q03940	Lys454	Rvb2p	Q12464	Lys338	154
Rvb1p	Q03940	Lys454	Rvb2p	Q12464	Ser339	164

Table S2 (continued). Intermolecular cross-linked residues, Related to STAR Method section “Lysine-specific cross-linking coupled with mass spectrometry”

Nop58p_447:R2TP Cross-links

Protein1	Accession Number	Cross-linked Residue	Protein2	Accession Number	Cross-linked Residue	Score
Pih1p	P38768	Lys52	Nop58p	Q12499	Lys393	188
Pih1p	P38768	Ser199	Nop58p	Q12499	Lys100	184
Pih1p	P38768	Lys233	Nop58p	Q12499	Lys411	150
Rvb1p	Q03940	Lys234	Nop58p	Q12499	Ser140	187
Rvb1p	Q03940	Lys174	Pih1p	P38768	Lys248	206
Rvb1p	Q03940	Lys177	Pih1p	P38768	Lys239	181
Rvb1p	Q03940	Lys177	Pih1p	P38768	Lys248	181
Rvb2p	Q12464	Lys414	Pih1p	P38768	Lys58	172
Rvb2p	Q12464	Thr417	Pih1p	P38768	Lys58	172
Pih1p	P38768	Lys293	Tah1p	P25638	Lys79	186
Rvb1p	Q03940	N-terminus	Rvb2p	Q12464	Lys128	187
Rvb1p	Q03940	Lys432	Rvb2p	Q12464	Lys59	182
Rvb1p	Q03940	Lys450	Rvb2p	Q12464	Lys331	218
Rvb1p	Q03940	Lys450	Rvb2p	Q12464	Lys338	212
Rvb1p	Q03940	Thr453	Rvb2p	Q12464	Lys331	158
Rvb1p	Q03940	Lys454	Rvb2p	Q12464	lys331	250
Rvb1p	Q03940	Lys454	Rvb2p	Q12464	Lys357	198
Rvb1p	Q03940	Lys454	Rvb2p	Q12464	Lys338	193
Rvb1p	Q03940	Lys454	Rvb2p	Q12464	Ser339	174